Platelet Membrane-Camouflaged Silver Metal-Organic Framework Drug System Against Infections Caused by Methicillin-Resistant *Staphylococcus Aureus*

Rong Huang
Central South University Third Xiangya Hospital
Guang-Qing Cai
Eighth Hospital of Changsha
Jian Li
Central South University Third Xiangya Hospital
Xi-Sheng Li
Central South University Third Xiangya Hospital
Hai-Ting Liu
Central South University Third Xiangya Hospital
Xue-Ling Shang
Central South University Third Xiangya Hospital
Jian-Dang Zhou
Central South University Third Xiangya Hospital
Xin-Min Nie (niexinmin@csu.edu.cn)
Central South University Third Xiangya Hospital https://orcid.org/0000-0003-3104-2505
Rong Gui
Central South University Third Xiangya Hospital

Research Article

Keywords: platelet, metal-organic framework, vancomycin, methicillin-resistant Staphylococcus aureus

Posted Date: May 5th, 2021

DOI: https://doi.org/10.21203/rs.3.rs-458558/v1

Version of Record: A version of this preprint was published at Journal of Nanobiotechnology on August 4th, 2021. See the published version at https://doi.org/10.1186/s12951-021-00978-2.

Abstract

Background

Due to the intelligent survival strategy and self-preservation of methicillin-resistant *Staphylococcus aureus* (MRSA), many antibiotics are ineffective in treating MRSA infections. Nano-drug delivery systems have emerged as a new method to overcome this barrier. The aim of this study was to construct a novel nano-drug delivery system for the treatment of MRSA infection, and to evaluate the therapeutic effect and biotoxicity of this system. We prepared a nano silver metal-organic framework using 2-methylimidazole as ligand and silver nitrate as ion provider. Vancomycin (Vanc) was loaded with Ag-MOF, and nano-sized platelet vesicles were prepared to encapsulate Ag-MOF-Vanc, thus forming the novel platelet membrane-camouflaged nanoparticles PLT@Ag-MOF-Vanc. The mice were infected with MRSA by tracheal injection to establish a model of pneumonia.

Results

The synthesized Ag-MOF particles had uniform size and shape of radiating corolla. The mean nanoparticle size and zeta potential of PLT@Ag-MOF-Vanc were 148 nm and − 25.6 mV, respectively. The encapsulation efficiency (EE) and loading efficiency (LE) of vancomycin were 81.0% and 64.7%, respectively. PLT@Ag-MOF-Vanc was shown to be a pH-responsive nano-drug delivery system with good biocompatibility. Ag-MOF had a good inhibitory effect on the growth of three common clinical strains (*Escherichia coli*, *Pseudomonas aeruginosa*, and *Staphylococcus aureus*). PLT@Ag-MOF-Vanc showed better antibacterial activity against common clinical strains in vitro than vancomycin alone. PLT@Ag-MOF-Vanc killed MRSA through multiple approaches, including interfering with the metabolism of bacteria, catalyzing reactive oxygen species production, destroying the integrity of cell membrane, and inhibiting biofilm formation. PLT@Ag-MOF-Vanc targeted the MRSA infected sites and effectively reduced the dosage of vancomycin with no obvious toxicity.

Conclusions

PLT@Ag-MOF-Vanc is a novel effective targeted drug delivery system, which is expected to be used safely in anti-infective therapy of MRSA.

Introduction

Staphylococcus aureus is a kind of gram-positive bacteria with strong pathogenicity. It can cause infections of the skin and soft tissues, and internal organs; it is also the most common gram-positive bacterial species that causes sepsis[1]. More severe cases may progress to multiple organ failure, diffuse intravascular coagulation, lactic acidosis, and even death. Antibiotics are the first-line drugs in bacterial infection treatment; however, due to the abuse of antibiotics and long-term natural selection of bacteria,

drug-resistant bacteria producing β-lactamase appeared, posing a major threat to the existing antibiotics in clinical practice[2]. At present, more than 90% of *S. aureus* clinical isolates are resistant to penicillin[3]. To overcome penicillin resistance, scientists developed methicillin, but within two years of using methicillin, in 1961, Jevons found methicillin-resistant *Staphylococcus aureus* (MRSA) for the first time in the UK. MRSA is resistant not only to methicillin, but also to all other β-lactams and cephalosporins with the same structure as methicillin[4].

MRSA can escape the clearance of the innate immune system and antibiotics with the help of various factors. Staphylococcal toxins, including α-toxin, β-toxin, δ-toxin, and PSMα, can lead to intracellular proliferation and transmission; moreover, they play a role in maintaining MRSA's intracellular survival mode[5]. Biofilm is formed under various factors and can facilitate the escape of antibiotics and the immune system[6]. In addition, the small colony variant (SCV) phenotype is a challenge in treating *S. aureus* infection because of its low metabolic level and lower virulence factor expression compared with normal phenotype[7]. A large number of antibiotics lack the ability to penetrate cell membranes and bacterial biofilm; moreover, their intracellular residence time is short, thus leading to insufficient intracellular distribution and low intracellular concentration, which makes the treatment of *S.s aureus* infection extremely challenging[8]. Due to the intelligent survival strategy and self-preservation of *S. aureus*, many antibiotics are ineffective in treating infections caused by MRSA. Indeed, MRSA strains are not only widely resistant to penicillin, macrolides, and fluoroquinolones, but they are also resistant to first-line drugs such as vancomycin and linazolid[9, 10], which greatly limits clinical treatment choices. Besides, high doses and prolonged use of vancomycin can cause severe ototoxicity and nephrotoxicity[11, 12].

In recent years, nanoparticle carriers have been reported as a potential strategy to effectively improve the permeability of the cell membrane for loaded drugs, enhance drug's intracellular accumulation, improve the antibacterial activity of antibiotics against drug-resistant strains, provide a variety of bactericidal mechanisms, and inhibit the formation of *Staphylococcus aureus* biofilm[8]. Metal-organic frameworks (MOFs) are polymers assembled by metal ions and organic ligands through coordination. Coordination polymers contain many metal ions and ligands and they have flexible structure and unique properties; moreover, they are organic–inorganic hybrid materials with high porosity and specific surface area[13]. Silver ion has good antibacterial activity. Therefore, in this study, we used 2-methylimidazole as a ligand and silver nitrate as an ion provider to prepare a nano metal-organic framework named Ag-MOF. Ag-MOF loaded with vancomycin was used to treat MRSA infection through a dual antibacterial mechanism.

In view of the short half-life of exogenous nanoparticles in the circulatory system, natural biofilm was used to camouflage nanoparticles in this study. Among natural biological carriers, platelets (PLT)—autologous blood cells—have good biocompatibility, with which synthetic carriers cannot compete[14]. Not only can platelet membrane-camouflaged nanoparticles significantly reduce the macrophage uptake and particle-induced complement activation, but also they still show platelet-like function after camouflaging, which can effectively solve the plasma protein absorption on nanomaterial surface[15, 16]. In addition, platelets are the first and most abundant cell type accumulated in the intravascular infection and have

the ability to recognize inflammatory cells[17, 18]. The inflammatory endothelial cells express P-selectin and E-selectin; the platelet membrane can express VWF, ICAM-1, and P-selectin receptor GPIBα, thus enabling platelets to bind with the inflammatory endothelial cells[19]. *S. aureus* can bind to platelets through adhesins such as protein A, agglutinin A, agglutinin B, fibronectin A, and serine-rich surface proteins [20, 21]. Using platelets to camouflage nanoparticles is expected to improve the short half-life of exogenous nanoparticles in the circulatory system; moreover, it can also target the inflammatory sites and *S. aureus* surface through platelet surface proteins, thereby inhibiting MRSA.

In this study, 2-methylimidazole was used as a ligand and silver ion was provided by silver nitrate to prepare the nano metal-organic framework Ag-MOF. Vancomycin was loaded with Ag-MOF, and nano-sized platelet vesicles were prepared to encapsulate Ag-MOF-Vanc, thereby forming the novel platelet membrane-camouflaged nanoparticles PLT@Ag-MOF-Vanc (Fig. 1). The PLT@Ag-MOF-Vanc synthesized in our study had a high drug loading rate, good biocompatibility, dual antibacterial mechanism, and targeting; it also has the ability to effectively improve the antibacterial activity of vancomycin and reduce the dosage of vancomycin.

Results And Discussion

Preparation and characterization of PLT@Ag-MOF-Vanc

As shown in Fig. 1, the preparation of PLT@Ag-MOF-Vanc mainly included the following three steps: 1) synthesis of Ag-MOF with 2-methylimidazole and $AgNO_3$ in a high temperature reactor; 2) loading vancomycin to Ag-MOF to synthesize Ag-MOF-Vanc; 3) adding platelet membrane vesicles to encapsulate Ag-MOF-Vanc to form the final product PLT@Ag-MOF-Vanc. Transmission electron microscopy (TEM) (Fig. 2a) showed that the synthesized Ag-MOF particles had uniform size (130–150 nm) and shape of radiating corolla. After the fusion with PLTm vesicles, Ag-MOF was observed to be encapsulated into PLTm vesicles. The protein composition of PLT membrane vesicles and PLT@Ag-MOF-Vanc was detected by sodium dodecyl sulfate polyacrylamide gel electrophoresis(SDS-PAGE). The results showed that PLT@Ag-MOF-Vanc and platelet membrane vesicles had similar protein profiles, which also confirmed the successful transfer of platelet membrane proteins to PLT@Ag-MOF-Vanc (Fig. 2b). Dynamic light scattering (DLS) data showed that the particle size of Ag-MOF was about 133 nm. After the encapsulation by PLT membrane vesicles, the particle size of PLT@Ag-MOF-Vanc was about 148 nm and was close to the size of PLT membrane vesicles (146 nm, Fig. 2c), which was comparable with the TEM results. Zeta potential of Ag-MOF, PLTm, and PLT@Ag-MOF-Vanc were − 19.0 mV, − 18.6 mV, and − 25.6 mV, respectively (Fig. 2d).

UV-vis spectrum analysis showed that PLT@Ag-MOF-Vanc had three characteristic absorption peaks, located at 199 nm, 213 nm, and 281 nm, which were consistent with the characteristic absorption peaks of PLT membrane vesicles, Ag-MOF, and vancomycin, respectively (Fig. 2e). FTIR results also showed that the infrared spectrum of Ag-MOF-Vanc contained the characteristic peaks of Ag-MOF and vancomycin (Fig. 2f).

Drug loading and release of PLT@Ag-MOF-Vanc

MOF is an ideal drug carrier due to its high porosity and specific surface area. In this study, vancomycin was loaded in Ag-MOF, and the encapsulation efficiency (EE) and loading efficiency (LE) of vancomycin were 81.0% and 64.7%, respectively (Fig. 3a). The ideal drug carrier should efficiently load the drug but also reach specific sites to achieve responsive release. The pH values of the infected site and intracellular environment were lower than those of healthy tissue and extracellular environment, respectively[8, 22]. Therefore, pH-sensitive nanoparticles could have a better inhibitory effect on the infection of *Staphylococcus aureus*. In order to verify the pH-responsive release of PLT@Ag-MOF-Vanc in infected microenvironment, pH 7.4 and pH 5.0 were used in this study to simulate neutral blood circulation environment and the acidic infection microenvironment, respectively. As shown in Fig. 3b, Vanc was more easily released at pH 5.0 than at pH 7.4. It is beneficial for Vanc in PLT@Ag-MOF-Vanc to be released at the infected site rather than in neutral circulation, indicating that PLT@Ag-MOF-Vanc can be used for drug delivery, especially at the infected site. Similar to Vanc, the release rate of Ag^+ in Ag-MOF increased with the decrease in pH value (Fig. 3c). In summary, Ag^+ and Vanc in PLT@Ag-MOF-Vanc can be released rapidly in the weak acidic environment of the infected area. In addition, the cumulative release rate of Ag^+ and Vanc in PLT@Ag-MOF-Vanc was lower than that in Ag-MOF-Vanc, indicating that PLT membrane inhibited the rapid release of the drug to some extent and played a role in continuous release. These results indicate that PLT@Ag-MOF-Vanc is an effective drug carrier.

Biocompatibility of PLT@Ag-MOF-Vanc

To evaluate whether PLT@Ag-MOF-Vanc was endowed with good blood compatibility after PLT membrane encapsulation, hemolysis test was performed. Namely, 5% erythrocytes were incubated with different concentrations of Ag-MOF and PLT@Ag-MOF (0, 5, 10, 20, 40, 80, and 160 μg/mL) for 2 h. As shown in Fig. 4a, Ag-MOF and PLT@Ag-MOF did not cause significant hemolysis during 2 h (less than 3% for both). In addition, the hemolysis rate induced by PLT@Ag-MOF was significantly lower than that of Ag-MOF, indicating that the encapsulation by PLT membrane increased PLT@Ag-MOF blood compatibility.

To demonstrate the immune escape ability of PLT membrane-camouflaged PLT@Ag-MOF-Vanc, the phagocytosis of RAW264.7 macrophages was evaluated by laser confocal fluorescence microscopy (LCFM). The green fluorescence of Ag-MOF was used for cell imaging. As shown in Fig. 4b, 24 hours after injection of Ag-MOF-Vanc, a large number of Ag-MOF without red PLT was engulfed by RAW264.7 cells. Meanwhile, under the same conditions, the green fluorescence in RAW264.7 cells treated with PLT@Ag-MOF-Vanc was significantly reduced; these data indicated that after being encapsulated by PLT membrane vesicles, the immunogenicity of PLT@Ag-MOF-Vanc decreased and was not recognized as a non-self-component by macrophages, so the phagocytosis was effectively inhibited. These above characteristics endow PLT@Ag-MOF-Vanc with prolonged circulatory half-life by reducing recognition and clearance by phagocytes from the reticuloendothelial system in vivo.

To further evaluate the cytotoxicity of the material, HeLa cells and HUVECs were treated with different concentrations (0, 5, 10, 20, 40, 80, and 160 ug/mL) of Ag-MOF and PLT@Ag-MOF, and the cell vitality was detected by CCK-8. As shown in Fig. 4c, after 48 h of mixed culture with the added material, cell vitality did not significantly decrease; therefore, Ag-MOF and PLT@Ag-MOF have no obvious cytotoxicity. In this study, the effects of the materials on cell apoptosis and reactive oxygen species (ROS) production were further detected by flow cytometry. Compared with the control group, the apoptosis rate and ROS production were not increased in Ag-MOF, Ag-MOF-Vanc, and PLT@Ag-MOF-Vanc groups (Fig. 4d and 4e). Apoptosis is a mechanism of cell death, and ROS is a key molecule in cell apoptosis and autophagy[23]. These results indicate that the synthesized material in this study does not lead to cell death by promoting apoptosis.

In vitro antibacterial effect of Ag-MOF-Vanc

In this study, the antibacterial effect of the newly synthesized Ag-MOF on three common clinical strains (*Escherichia coli* ATCC25922, *Pseudomonas aeruginosa* ATCC27853, and *Staphylococcus aureus* ATCC25923) was investigated by disc method. The results of antibacterial zone showed that Ag-MOF had a good inhibitory effect on the growth of the three strains (Fig. 5a and 5b). For MRSA (ATCC25923), the MIC of Ag-MOF was 8 μg/mL (Fig. 5c). The antibacterial effects of vancomycin alone and Ag-MOF-Vanc on MRSA were compared; the results showed that the antibacterial zone of Ag-MOF-Vanc was larger than that of vancomycin alone at different concentrations (Fig. 5d). The MIC of vancomycin alone was 2 μg/mL; in contrast, the MIC of Ag-MOF-Vanc was 0.5 μg/mL (Fig. 5e), which was only about one fourth of that of vancomycin alone. The above results indicate that Ag-MOF could enhance the antibacterial effect of Vanc against MRSA and reduce the dosage of vancomycin.

When MRSA was exposed to different concentrations (0, 10, 20, 40 μg/mL) of Vanc and Ag-MOF-Vanc for 1 h, the number of dead bacteria increased in a dose-dependent manner, suggesting that the antibacterial activity of Ag-MOF-Vanc was concentration-dependent (Fig. 5f). MRSA was treated with 5 μg/ mL Vanc and Ag-MOF-Vanc. The permeability of the bacteria increased with prolonged time, suggesting the time dependence of Ag-MOF-Vanc (Fig. 5g).

Antibacterial mechanism of PLT@Ag-MOF-Vanc

A series of studies were conducted to explore the antibacterial mechanism of PLT@Ag-MOF-Vanc. The first step for PLT@Ag-MOF-Vanc to exert its antibacterial effect is to target MRSA with the assistance of PLT membrane. In order to clarify the interaction between PLT@Ag-MOF-Vanc and MRSA, Ag-MOF-Vanc and PLT@Ag-MOF-Vanc at a certain concentration were co-incubated with MRSA for 3 h and observed by Scanning electron microscopy (SEM). Figure 6a shows that the surface of MRSA was relatively smooth when exposed to Ag-MOF-Vanc, while a large number of nanoparticles were attached to the surface after the exposure to PLT@Ag-MOF-Vanc. This indicates that PLT membrane promotes the binding of PLT@Ag-MOF-Vanc to MRSA and has a certain targeting effect.

To evaluate the effect of PLT@Ag-MOF-Vanc on bacterial metabolism, intracellular ATP levels were measured. The results showed that PLT@Ag-MOF-Vanc led to a significant decrease in ATP level, which

was significantly greater than that caused by Ag-MOF and Vanc (Fig. 6b). The decrease in ATP levels may be attributed to the inactivation of F-type ATP synthase(F-ATPase) (Fig. 6c). The functions of F-ATPase include catalyzing the synthesis of ATP in the last step of oxidative phosphorylation, working in reverse as an ATPase to produce the transmembrane proton electrochemical gradient required for molecular transport[24]. PLT@Ag-MOF-Vanc can significantly decrease the activity of F-ATPase.

The death of bacteria exposed to nanoparticles can be attributed to the disruption of energy production caused by the decoupling of oxidized phosphate in the cellular respiratory chain, the interference in membrane permeability, and the loss of enzyme activity involved in key metabolic pathways; among them, the excessive ROS production by cells is the most effective component for triggering bacterial cell death[25]. Therefore, it is very important to study the effect of nanoparticles on the formation of ROS in bacterial cells. We used 2,7-dichlorodihydrofluorescein diacetate (DCFH-DA) method to quantitatively detect ROS. Figure 6d shows the ROS production level of MRSA after the treatment with Ag-MOF, vancomycin alone, Ag-MOF-Vanc, and PLT@Ag-MOF-Vanc. Compared with the control group and the vancomycin alone group, Ag-MOF treatment significantly increased ROS levels. The variation was more obvious in the bacteria treated with Ag-MOF-Vanc and PLT@ Ag-MOF-Vanc. High ROS levels were observed in PLT@Ag-MOF-Vanc-treated bacteria, indicating that PLT@Ag-MOF-Vanc effectively bound to the bacterial surface, thus releasing a high proportion of silver ions in the target cells.

One of the main consequences of intracellular ROS accumulation is the damage to the membrane integrity caused by the gradual establishment of oxidative stress. In addition, nanoparticles can also cause physical damage to the cell membrane. Therefore, we continued to use malondialdehyde (MDA) method to detect cell lipid peroxidation to determine the degree of membrane damage. There were significant differences in MDA content among bacteria in different treatment groups (Fig. 6e). Compared with vancomycin alone, the content of MDA in PLT@Ag-MOF-Vanc-treated cells increased significantly. These results suggest that the interaction between Ag-MOF and bacterial surface increases the degree of bacterial damage.

One of the reasons for drug resistance and poor therapeutic effect of antibiotics is the generation of biofilms. Because of their high permeability, nanoparticles can penetrate thick biofilms. We speculated that Ag-MOF-Vanc may have a good inhibitory and scavenging effect on *Staphylococcus aureus* biofilm. During the early- and mid-stages during biofilm formation, two assays, crystal violet staining and the 2,3-bis (2-methoxy-4-nitro-5-sulfophenyl)-2H-tetrazolium-5-carbox-anilide (XTT) assay, are regarded as crucial experimental tools. The results of crystal violet staining and XTT staining after treating the MRSA biofilm with different drugs showed that PLT@Ag-MOF-Vanc effectively destroyed the biofilm formed by MRSA, and the effect was obviously better than that of Ag-MOF and vancomycin alone (Fig. 4f and 4h). The results obtained by confocal laser scanning microscopy were identical to those obtained by crystal violet and XTT analysis (Fig. 4g).

In conclusion, PLT@Ag-MOF-Vanc can kill MRSA through a comprehensive physical and chemical mechanism, including targeting MRSA via PLT membranes; interfering with the intracellular metabolism

of bacteria; catalytic production of ROS; damage to cell membrane integrity; and inhibiting the formation of biofilm.

Distribution of Intravenously Injected PLT@ Ag-MOF-Vanc

To demonstrate that PLT@Ag-MOF-Vanc can target the MRSA-infected sites in vivo, biodistribution in MRSA pneumonia model mice was evaluated by Small Animal In Vivo Imaging at 6, 24, and 48 h after Ag-MOF-Vanc and PLT@Ag-MOF-Vanc tail vein injection. As shown in Fig. 7a, Ag-MOF-Vanc rarely aggregated at the infected site within 48 h after injection, while PLT@Ag-MOF-Vanc mostly accumulated at the infected site. Then, 48 h after injection, the mice were killed by cervical dislocation, and fluorescence imaging of the heart, liver, spleen, lung, and kidney was performed in vitro (Fig. 7b). There was a small amount of Ag-MOF-Vanc aggregation in the lung, liver, and spleen; the accumulation of PLT@Ag-MOF-Vanc in the lung was much higher than that of Ag-MOF-Vanc. The above results indicate that PLT@Ag-MOF-Vanc has a good targeting effect on the MRSA-infected sites in vivo.

Anti-infection effect of PLT@Ag-MOF-Vanc in vivo

The present study further evaluated the anti-infection effect of PLT@Ag-MOF-Vanc in vivo in the MRSA pneumonia model of Kunming mice. The infected mice were divided into the following five groups: normal saline group, Ag-MOF group, Vanc group, Ag-MOF-Vanc group, and PLT@Ag-MOF-Vanc group. After establishing the model, the corresponding drugs were injected daily, and every day one mouse was taken from each group for Hematoxylin-eosin(HE) staining so as to observe the alveolar structure and integrity of ciliated endothelial cells, inflammation, necrosis, and infiltration by inflammatory cells (macrophages) in the alveoli. The results showed significantly better improvement rate of the lung condition in PLT@Ag-MOF-Vanc group compared with other groups, and the alveoli recovered from the third day of the treatment, with no obvious inflammatory cell infiltration (Fig. 8a). Four days after the treatment, the levels of inflammatory cytokines IL-6 and TNF-α in the lung tissue of mice were examined by immunohistochemical staining; the results showed that the expression levels of IL-6 and TNF-α in the normal saline group, Ag-MOF group, Vanc group, and Ag-MOF-Vanc group were still significantly higher compared with the normal control mice, while those in PLT@Ag-MOF-Vanc group almost returned to normal control level (Fig. 8b). In addition, blood was taken for hematological tests; the results showed that the WBC and neutrophil (NEU) count and inflammatory marker CRP level were significantly reduced in the PLT@Ag-MOF-Vanc group (Fig. 8c). The levels of IL-6 and TNF-α in blood were examined by ELISA; it was shown that the level of inflammatory cytokines significantly decreased in the PLT@Ag-MOF-Vanc group (Fig. 8c). The bacterial count in alveolar lavage fluid of different treatment groups also showed that the number of residual bacteria was the lowest after the treatment with PLT@Ag-MOF-Vanc (Fig. 8d). After 5 days of treatment, the survival rate of mice in the PLT@Ag-MOF-Vanc group was 100%, while death occurred in other groups (Fig. 8e). All the above results show that PLT@Ag-MOF-Vanc has a good anti-infective effect, which is significantly superior to Vanc alone and Ag-MOF or uncoated Ag-MOF-Vanc, indicating that Ag-MOF and Vanc have a synergistic anti-infective effect. Meanwhile, after encapsulation with platelet membrane, Ag-MOF-Vanc could be targeted and transported to the MRSA-infected site, thus further strengthening the anti-infective effect of PLT@Ag-MOF-Vanc.

In vivo toxicity assessment of PLT@Ag-MOF-Vanc

In order to evaluate the potential toxicity of PLT@Ag-MOF-Vanc, hematological indicators of normal mice were measured 1 week after the tail vein drug injection. We measured complete blood counts(red blood cell (RBC), white blood cell (WBC), platelet (PLT)), liver function indicators (alanine transaminase (ALT), aspartate aminotransferase (AST)), and renal function indicators (blood urea nitrogen (BUN), and creatinine (CREA)). There was no significant difference in any of these indicators among different groups (Fig. 9a), indicating that PLT@Ag-MOF-Vanc had no significant effect on the production of red blood cells, white blood cells, and platelets in blood, and it had no obvious hepatorenal toxicity.

To further clarify the in vivo toxicity of PLT@Ag-MOF-Vanc, we used HE staining to evaluate the pathological changes in major organs (heart, liver, spleen, lung, and kidney). The results showed that PLT@Ag-MOF-Vanc did not cause significant damage to the heart, liver, spleen, lung, and kidney; it had low toxicity in vivo and good biocompatibility (Fig. 9b).

Conclusion

In this study, we designed and synthesized a platelet membrane-camouflaged nano-drug delivery system (PLT@Ag-MOF-Vanc). The drug release and silver ion release of PLT@Ag-MOF-Vanc were shown to be pH-responsive, which can prevent the delivery system from prereleasing drugs in the circulatory system. The platelet membrane on PLT@Ag-MOF-Vanc effectively covers the internal nano-core, reduces the recognition and clearance of reticuloendothelial system such as liver and spleen, and has good biocompatibility. Ag-MOF-Vanc showed good antibacterial activity against common clinical strains in vitro, significantly better than vancomycin alone. In the MRSA pneumonia model, PLT@Ag-MOF-Vanc targeted the MRSA-infected sites. Combining the antibacterial ability of Ag-MOF with Vanc, the growth of MRSA was inhibited and the effect was better than when using vancomycin alone; in that way, the required dosage of vancomycin was effectively reduced, with no obvious organ toxicity. PLT@Ag-MOF-Vanc is a novel and effective targeted drug delivery system that can be used for safe and effective anti-infection therapy.

Materials And Methods

Materials

Silver nitrate and 2-methylimidazole were purchased from Aladdin (China). Cy5 and Hoechst 33342 were provided by Yeasen Biotechnology (China) Co., Ltd. Dialysis membrane (2 kD) was purchased from SolarBio (China). Annexin V-FITC/PI Apoptosis assay Kit and ROS assay Kit were provided by Beyotime Biotechnology (China). Cell Counting Kit-8 (CCK-8) was manufactured by Dojindo Laboratories, Japan. Primary antibodies against TNF-α and IL-6 monoclonal antibodies were purchased from Proteintech (China). Viability/Cytotoxicity Assay for Bacteria Live & Dead Cells was purchased from US Everbright Inc. (USA).

Cells and mice

HeLa, HUVEC, and RAW264.7 cells were bought from the Advanced Research Center, Central South University; they were cultured in RPMI-1640 medium supplemented with 10% fetal bovine serum. The cells were kept at 37°C in 5% CO_2 at atmospheric pressure. Kunming mice (male, 6 weeks old) were bought from Hunan SJA Laboratory Animal Co., Ltd.

Synthesis of Ag-MOF

First, 1 g 2-methylimidazole was dissolved in 10 mL ddH_2O; 57 mg silver nitrate was dissolved in 2 mL ddH_2O; then, the silver nitrate solution was dropped into the 2-methylimidazole aqueous solution. The solution was placed in a polyethylene reaction pot at 120°C for 15 min, washed 2–3 times using ddH_2O, and centrifuged at 14,000 rpm for 10 min.

Synthesis of Ag-MOF-Vanc

We dissolved 0.5 mg Ag-MOF in 1 mL ddH_2O; 5.2 μg vancomycin was added, stirred overnight at room temperature by magnetic force, and Ag-MOF-Vanc was obtained by centrifugation.

Preparation of PLT membranes (PLTm) vesicles

The whole blood of female Kunming mice was used and placed in tubes containing heparin. Platelets were isolated from whole blood by centrifugation and washing. PLTm were extracted by repeated freeze–thaw extraction, suspended in phosphate-buffered brine (PBS), and then subjected to ultrasonic treatment (2 min, 42 kHz, 100 W) to produce PLTm vesicles.

Construction of PLT@Ag-MOF-Vanc

PLTm vesicles were fused with equal volume of Ag-MOF-Vanc by ultrasound (5 min, 42 kHz, 100 W). The sample was filtered 20 times using a porous syringe filter with a membrane pore diameter of 200 nm and centrifuged (2500 rpm, 10 min) to remove the excess PLTm to separate PLT@Ag-MOF-Vanc.

Characterization

PLT@Ag-MOF-Vanc was observed through TEM with Tecnai G2 Spirit TEM (FEI, USA). PLTm-encapsulated nanoparticles were detected and their size was determined. Zetasizer Nano ZS (Malvern Nano Series, Malvern, UK) was used to evaluate the surface charge. The platelet membrane proteins were identified by SDS-PAGE. The absorption spectra of Ag-MOF-Vanc were obtained using UV-vis (Scandrop, Analytik Jena, Germany). The molecular functional groups of Ag-MOF-Vanc were studied by Fourier-transform infrared spectroscopy (FTIR).

Determination of EE and LE

We dissolved 0.5 mg Ag-MOF in 1 mL ddH_2O, and 5.2 μg vancomycin was added and stirred overnight by magnetic stirring at room temperature. Ag-MOF-Vanc was obtained by centrifugation. The maximum absorbance of vancomycin was determined by UV-vis spectrophotometry. The standard concentration

gradient was set and the standard curve of concentration and absorbance was established; then, we calculated the uncombined vancomycin in the supernatant. The calculation formulas for LE and EE were as follows:

EE = (quality of drugs contained on nano-carrier/ total amount of drugs used) × 100%,

LE = (mass of drug contained on nano-carrier/ mass of nano-carrier) × 100%.

Release of vancomycin and silver ion

In vitro drug release experiments were carried out under pH 7.4 and pH 5.0 to observe whether PLT@Ag-MOF-Vanc could release vancomycin and silver ion more easily under acidic environment. Next, 2 mL PLT@Ag-MOF-Vanc was put into a 2kD dialysis bag and immersed in 20 mL PBS solution at pH 7.4 and pH 5.0, seperately. The absorbance of vancomycin in dialysate was determined at 280 nm. Cumulative release of vancomycin was based on the standard curve. The concentration of Ag^+ in dialysate was determined by a direct-reading inductively coupled plasma emission spectrometer (Spectro Blue, Spectro, Germany).

Biocompatibility of PLT@Ag-MOF-Vanc

The biocompatibility of PLT@Ag-MOF-Vanc was evaluated by hemolysis rate and macrophage phagocytosis test. PLT@Ag-MOF-Vanc specimens of different concentrations (0.25–2.0 mg/mL) were mixed with 5% Kunming mice erythrocyte suspension, incubated at 37°C for 2 h, and centrifuged at 3500 rpm for 5 min. The absorbance was obtained at 545 nm using ultra-pure water and PBS as positive and negative controls, respectively. The evaluation formula of hemolysis rate was as follows: hemolysis rate (%) = (absorbance of experimental sample − absorbance of negative control)/(absorbance of positive control − absorbance of negative control) × 100. To determine the immune escape ability of PLT@Ag-MOF-Vanc, RAW264.7 cells were inoculated in a 6-well plate (about 3×10^5 cells/well) and incubated for 24 h. PLT@Ag-MOF-Vanc and Ag-MOF-Vanc were added and incubated for 24 h and then stained with Hoechst 33342. The phagocytosis and fluorescence signals of macrophages against PLT@Ag-MOF-Vanc were obtained under LCFM (TCS SP8 CARS, Leica, Germany).

The cytotoxicity of PLT@Ag-MOF-Vanc was evaluated using HeLa cells and HUVECs. The cells were inoculated in 96-well plate (2×10^3 cells/well) and incubated for 24 h. The concentrations of Ag-MOF-Vanc and PLT@Ag-MOF-Vanc were calculated with the concentration of Vanc as 2.0 μg/mL. After incubation for 48 h, CCK-8 solution (10 μL) was added to each well for 3 h, and the absorbance was measured at 450 nm.

Cell apoptosis was detected by Annexin V-FITC/PI apoptosis detection kit. In brief, the cells were inoculated at 10^6 cells/bottle in T25 culture containers and incubated for 24 h until the cells adhered to the wall. Ag-MOF-Vanc and PLT@Ag-MOF-Vanc were added for further incubation for 48 h. Apoptosis was detected by flow cytometry as per standard procedures of the Annexin V-FITC/PI Apoptosis Detection Kit.

The production of ROS was detected. The cells were inoculated at 10^6 cells/bottle in T25 culture containers and incubated for 24 h until the cells adhered to the wall, and the remaining treatment was the same as before. The concentrations of Ag-MOF-Vanc and PLT@Ag-MOF-Vanc were calculated with the concentration of Vanc as 2.0 μg/mL. After additional incubation for 48 h, the intracellular ROS were analyzed by flow cytometry in accordance with the standard operation of the ROS detection kit.

In vitro antibacterial experiment

Disc diffusion method

After single bacterial colony was obtained, the concentration of the bacterial solution was adjusted to 0.5 MCF with normal saline, and the bacterial solution was evenly spread on Mueller-Hinton (MH) medium. After placing a paper on the staining medium, different concentrations of the Ag-MOF, Vanc, or Ag-MOF-Vanc were injected into the paper. After incubation for 1 day, the inhibition zone was observed.

Dilution method

First, we took one to two MRSA colonies and added them to PBS solution for dilution. Then, we added them to the Luria-Bertani (LB) culture medium so that the final concentration of the bacteria was 5×10^5 CFU/mL. We added a higher concentration of the drug and 200 μL bacterial solution mentioned above to the first row of a 96-well plate. We added 100 μL bacterial solution to the remaining row of the 96-well plate without antibiotics. Then, we evenly mixed the bacterial solution containing antibiotics in the first row and took out 100 μL and added into the second row. We mixed the solution in the second row evenly, then extracted 100 μL to the third row, and so on. Then, the 96-well plate was placed in the incubator for 16–20 h, and the absorption at 600 nm was read with a microplate reader to determine the minimum inhibitory concentration.

Staining of live and dead bacteria

DMAO/EthD- III and other dyes were mixed with the bacteria solution to be tested in a certain proportion. They were mixed well and incubated in the dark at room temperature for 15 min. Next, 5-μL stained bacterial suspension droplets were placed on a glass slide with an 18-mm square cover glass and observed by Confocal laser scanning microscope (CLSM, Zeiss LSM 800, Germany). Live (green fluorescence) and dead (red fluorescence) bacteria were observed using FITC and CY3 channels, respectively.

Antibacterial mechanism-related experiments

ATP and F-ATPase

Logarithmic growth MRSA (1×10^6 CFU) was collected and resuspended in PBS buffer (pH = 7.4). Different drugs were added to the bacteria and cultured at 37°C for 6 h. The bacteria were divided, and the supernatant was collected after centrifugation at 1000 g. Then, the ATP level was determined using the

ATP kit (Beyotime Biotechnology, China), and the F-ATPase activity was detected by F-ATPase activity kit (GenMed Scientifics, Shanghai, China).

ROS

Logarithmic growth MRSA (1×10^6 CFU) was collected and resuspended in PBS buffer (pH = 7.4). After ROD staining, different drugs were added and incubated at 37°C for 1 h. Fluorescence was detected by flow cytometry.

MDA

Ag-MOF, Vanc, Ag-MOF-Vanc, or PLT@Ag-MOF-Vanc were co-incubated with bacteria, centrifuged (12,000 rpm, 2 min), resuspended in 1 mL of 2.5% freshly configured trichloroacetic acid (TCA), and then centrifuged (12000 rpm, 20 min, 4°C). The supernatant was diluted with 5% thiobarbituric acid; the same volume of TCA was added, and the mixture was heated in 100°C water bath for 30 min, followed by centrifuge (12000 rpm, 20 min, 4°C). We determined the absorbance at 532 nm and calculated MDA content (pg/mL) with a molar extinction coefficient of 1.56 $nM^{-1}cm^{-1}$.

Biofilm detection

CLSM

One hundred microliters of drug culture solution was added to each well in the fluorescent confocal plate; 100 μl of overnight cultured bacteria solution was inoculated and incubated at 37°C for 24 h. After washing the plate for three times with PBS, we added DMAO/EthD- III dye and incubated at 37°C in dark for 20 min. After washing with PBS for three times and drying, we collected pictures with CLSM.

Crystal violet staining

We added 100 μl of drug culture solution to each well of the 96-well plate; 100 μl of overnight cultured bacteria solution was inoculated and incubated at 37°C for 24 h. After washing with PBS for three times, the plate was fixed with methanol. Excess methanol was sucked out; after drying at room temperature, we added 200 μl 1% crystal violet solution and incubated at room temperature for 15 min. The excess dye was sucked out and washed with PBS for 2–3 times. After drying at room temperature, 200 μl 95% ethanol was added and incubated for 20 min. The absorbance value was determined at 570 nm.

XTT dyeing

XTT with a concentration of 0.2 mg/mL was prepared with PBS, and then the XTT solution was volumized with phenazine methyl ester to a concentration of 0.02 mg/mL. Next, 100 μL of drug culture solution was added to each well of the 96-well plate; 100 μL of overnight cultured bacteria solution was inoculated and incubated at 37°C for 24 h. After washing the plate with PBS for three times, XTT solution was added and incubated at 37°C for 3 h, and the absorbance value was determined at 490 nm.

Study on the targeting ability of PLT@Ag-MOF-Vanc

SEM

Ag-MOF-Vanc and PLT@Ag-MOF-Vanc were mixed with bacteria for 3 h and fixed at room temperature with 2.5% glutaraldehyde, 2.5% paraformaldehyde, and 0.1 M calcium carbonate buffer solution dissolved in deionized water for 2 h. Cover slides were prepared with one drop of 1% polylysine to capture the cells. We placed one drop of the fixed medium on the cover glass and incubated with water for 5 min before rinsing. The sample was then dehydrated with a series of ethanol concentrations (25%, 50%, 75%, and 95%) and washed three times in 100% ethanol. The sample was air-dried for about 24 h, then coated with Au and Pd (7 nm thick) on the biofilm, and observed by SEM(Quanta 250FEG, USA).

In vivo imaging

To evaluate the targeting ability of PLT@Ag-MOF-Vanc in vivo, Kunming mice were injected with Cy5-labeled Ag-MOF-Vanc or Cy5-labeled PLT@Ag-MOF-Vanc through the tail vein. The Xenogen IVIS Lumina XR imaging system (Caliper Life Sciences, USA) was used to evaluate fluorescence signals at 6, 24, and 48 h after administration. After 48 h, the mice were killed by cervical dislocation; the brain, heart, liver, spleen, lung, and kidney were collected. The fluorescence signal was further detected using the Xenogen IVIS Lumina XR imaging system (Caliper Life Sciences, USA).

Mice model of MRSA pneumonia

Fifty male Kunming rats were randomly divided into five groups: normal saline group, Ag-MOF group, Vanc group, Ag-MOF-Vanc group, and PM@Ag-MOF-Vanc group. The mice were infected with 150 μL MRSA (concentration $1 \cdot 10^8$/mL) by tracheal injection. Eight hours after bacterial injection, the mice were given tail vein injection once a day. HE staining of lung tissue was taken on the first, second, third, and fourth day of treatment to observe the alveolar structure and integrity of ciliated endothelial cells, inflammation, necrosis, and infiltration of inflammatory cells (macrophages) in the alveoli. On day 4, the lung tissues were stained by immunohistochemistry to detect the expression of inflammatory cytokines TNF-α and IL-6. The bacterial count of bronchoalveolar lavage fluid was detected. The whole blood of the mice was collected for blood test indicators (complete blood count, CRP). The levels of TNF-α and IL-6 in blood were detected by ELISA. We recorded the survival status of mice and created the survival curve.

In vivo toxicity testing

Kunming mice weighing about 20 g were chosen and injected with 100 μL of different drugs (specific drugs and concentrations) via the tail vein. One week later, we collected whole blood to test hematological and biochemical indicators (RBC, WBC, PLT, ALT, AST, BUN, CREA). The mice were killed through cervical dislocation. The major organs (heart, liver, spleen, lung, and kidney) were collected, stained with HE, and observed and photographed under microscope.

Statistical Analysis

Data were assessed by SPSS 20.0 and expressed as mean ± SD. Intergroup differences were assessed by oneway ANOVA with subsequent Tukey's post-test.. Significance was demonstrated by $p < 0.05$.

Declarations

Acknowledgements

Not applicable

Funding

This project was supported by the National Natural Science Foundation of China (81602801, 81971748) and the Natural Science Foundation of Hunan Province (2019JJ40464).

Authors' contributions

XMN, RG, and RH designed the study. RH, HTL, XSL, JDZ, and JL performed

the laboratory correlative experiments. JL analyzed data. RH wrote the manuscript. XLS and XSL edited the manuscript. All authors read and approved the final manuscript.

Availability of data and materials

All data generated or analysed during this study are included in this published article.

Ethics approval and consent to participate

Animal experiments were approved by the Experimental Animal Welfare Ethics Committee of Central South University (No. 2020sydw0109).

Consent for publication

Not applicable.

Competing interests

The authors declare that they have no competing interests.

References

1. Thomer L, Schneewind O, Missiakas D. Pathogenesis of Staphylococcus aureus Bloodstream Infections. Annu Rev Pathol. 2016;11(1):343–64.
2. Bush K, Bradford PA. Epidemiology of β-Lactamase-Producing Pathogens. Clin Microbiol Rev. 2020;33(2):e00047-19.
3. Peacock SJ, Paterson GK. Mechanisms of Methicillin Resistance in Staphylococcus aureus. Annu Rev Biochem. 2015;84:577–601.
4. Gauguet S, D'Ortona S, Ahnger-Pier K, Duan B, Surana NK, Lu R,et al. Intestinal Microbiota of Mice Influences Resistance to Staphylococcus aureus Pneumonia. Infect Immun. 2015:4003–14.

5. Martin F, Bhanu S. Intracellular staphylococcus aureus: Live-in and let die. Front Cel Infect Microbiol. 2012;2:43.
6. Devlin H, Fulaz S, Hiebner DW, O'Gara JP, Casey E. Enzyme-Functionalized Mesoporous Silica Nanoparticles to Target and Disperse Biofilms. Int J Nanomed. 2021;16:1929–42.
7. Proctor R. Respiration and Small Colony Variants of Staphylococcus aureus. Microbiol Spectr. 2019;7(3): 10.1128/microbiolspec.GPP3-0069-2019.
8. Zhou K, Chao L, Chen D, Pan Y, Xie S. A review on nanosystems as an effective approach against infections of Staphylococcus aureus. Int J Nanomed. 2018;13:7333–47.
9. Gardete S, Tomasz A. Mechanisms of vancomycin resistance in Staphylococcus aureus. J Clin Invest. 2014;124(7):2836–40.
10. Wei H, Mao F, Ni S, Chen F, Li B, Qiu X, et al. Discovery of novel piperonyl derivatives as diapophytoene desaturase inhibitors for the treatment of methicillin-, vancomycin- and linezolid-resistant Staphylococcus aureus infections. Eur J Med Chem. 2018;145:235–51.
11. Bruniera FR, Ferreira FM, Saviolli LRM, Bacci MR, Feder D, da Luz Gonçalves Pedreira M, et al. The use of vancomycin with its therapeutic and adverse effects: a review. Eur Rev Med Pharmacol Sci. 2015;19(4):694–700.
12. Shime N, Saito N, Bokui M, Sakane N, Kamimura M, Shinohara T, et al. Clinical outcomes after initial treatment of methicillin-resistant Staphylococcus aureus infections. Infect Drug Resist. 2018;11:1073–81.
13. Wieme J, Lejaeghere K, Kresse G, Van Speybroeck V. Tuning the balance between dispersion and entropy to design temperature-responsive flexible metal-organic frameworks. Nat Commun. 2018;9(1):4899.
14. Dehaini D, Wei X, Fang RH, Masson S, Zhang L. Erythrocyte-Platelet Hybrid Membrane Coating for Enhanced Nanoparticle Functionalization. Adv Mater. 2017;29(16):1606209.
15. Hu CM, Fang RH, Wang KC, Luk BT, Thamphiwatana S, Dehaini D, et al. Nanoparticle biointerfacing by platelet membrane cloaking. Nature. 2015;526(7571):118–21.
16. Wei X, Gao J, Fang RH, Luk BT, Kroll AV, Dehaini D, et al. Nanoparticles camouflaged in platelet membrane coating as an antibody decoy for the treatment of immune thrombocytopenia. Biomaterials. 2016;111:116–23.
17. Yeaman MR. Platelets in defense against bacterial pathogens. Cell Mol Life Sci. 2010;67(4):525–44.
18. Vieira-de-Abreu A, Campbell RA, Weyrich AS, Zimmerman GA. Platelets: versatile effector cells in hemostasis, inflammation, and the immune continuum. Semin Immunopathol. 2012;34(1):5–30.
19. Mcfadyen JD, Kaplan ZS. Platelets Are Not Just for Clots. Transfus Med Rev. 2015;29(2):110–19.
20. Viela F, Prystopiuk V, Leprince A, Mahillon J, Speziale P, Pietrocola G, et al. Binding of Staphylococcus aureus Protein A to von Willebrand Factor Is Regulated by Mechanical Force. mBio. 2019;10(2):e00555-19.

21. Fitzgerald JR, Foster TJ, Cox D. The interaction of bacterial pathogens with platelets. Nat Rev Microbiol. 2006;4(6):445–57.
22. Pei Y, Mohamed MF, Seleem MN, Yeo Y. Particle engineering for intracellular delivery of vancomycin to methicillin-resistant Staphylococcus aureus (MRSA)-infected macrophages. J Control Release. 2017;267:133–43.
23. Su LJ, Zhang JH, Gomez H, Murugan R, Hong X, Xu D, et al. Reactive Oxygen Species-Induced Lipid Peroxidation in Apoptosis, Autophagy, and Ferroptosis. Oxid Med Cell Longev. 2019;2019:5080843.
24. Cui Y, Zhao Y, Tian Y, Zhang W, Lü X, Jiang X. The molecular mechanism of action of bactericidal gold nanoparticles on Escherichia coli. Biomaterials. 2012;33(7):2327–33.
25. Medina Cruz D, Mi G, Webster TJ. Synthesis and characterization of biogenic selenium nanoparticles with antimicrobial properties made by Staphylococcus aureus, methicillin-resistant Staphylococcus aureus (MRSA), Escherichia coli, and Pseudomonas aeruginosa. J Biomed Mater Res A. 2018;106(5):1400–12.

Figures

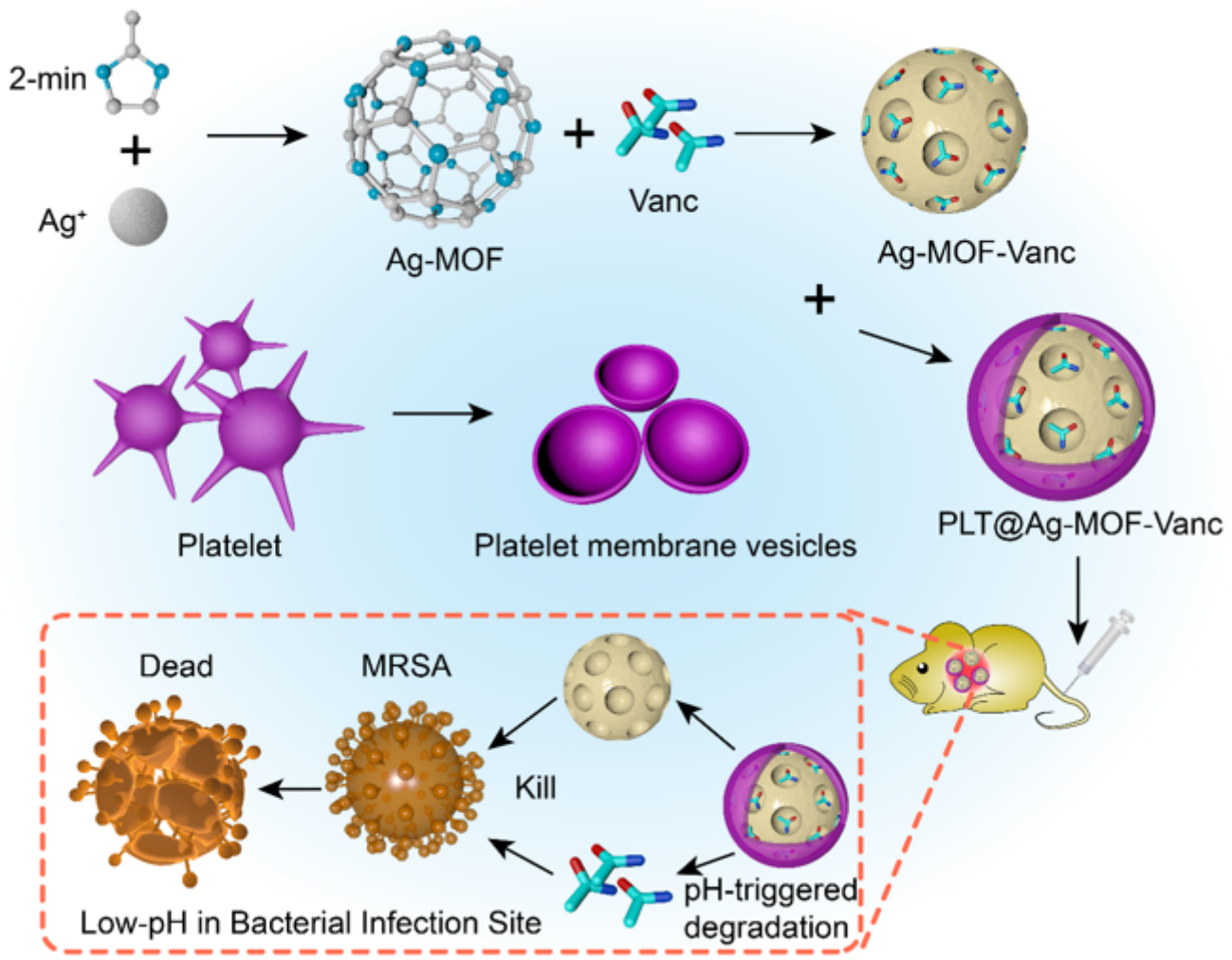

Figure 1

Schematic diagram of PLT@Ag-MOF-Vanc in the treatment for MRSA infection

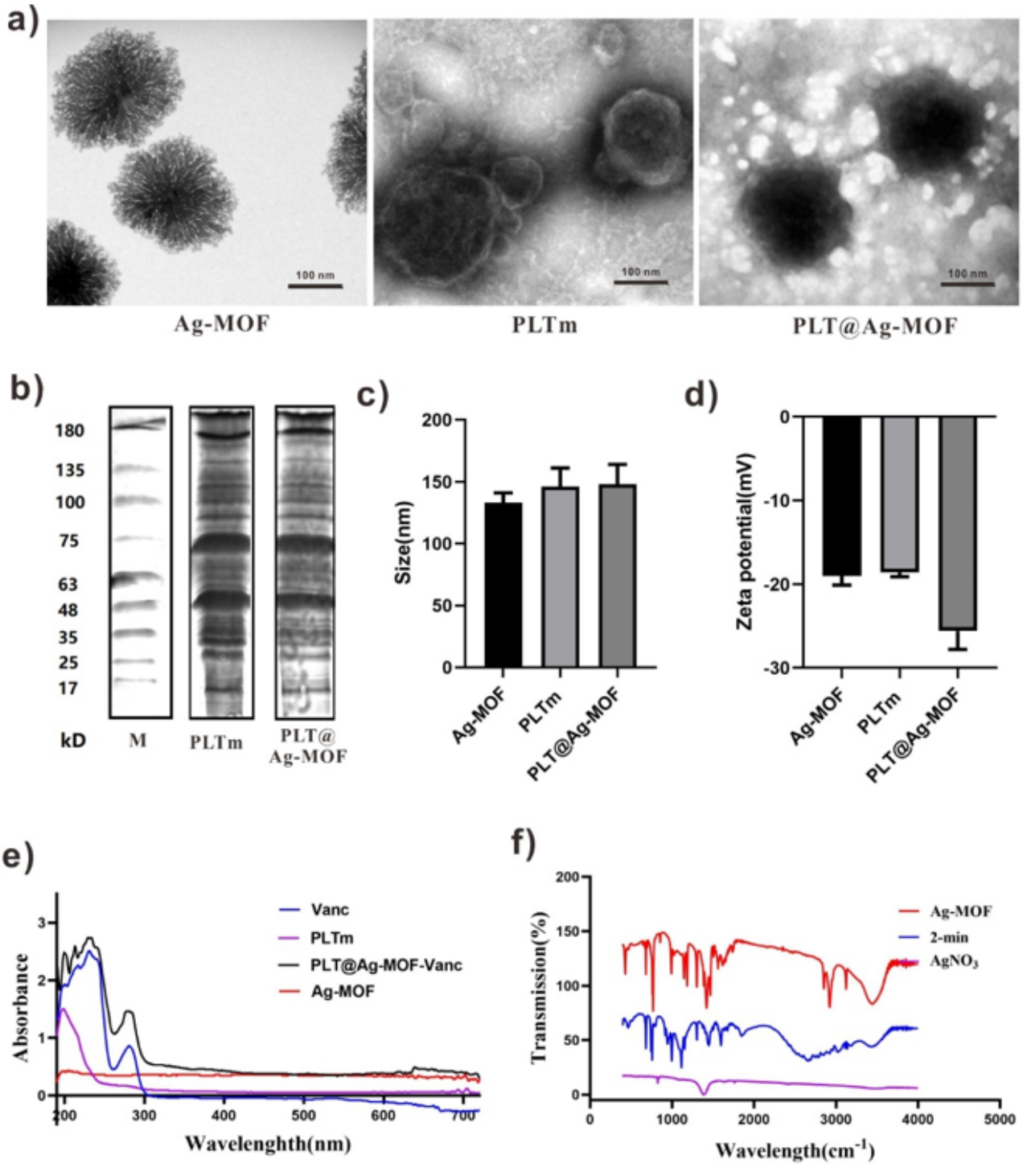

Figure 2

Characterization of PLT@Ag-MOF-Vanc. (a) TEM images of Ag-MOF, PLTm, and PLT@Ag-MOF. (b) SDS-PAGE protein assessment. (c) Particle sizes and (d) zeta potential values of Ag-MOF, PLTm, and PLT@Ag-

MOF. (e) UV-vis spectra of Vanc, Ag-MOF, PLTm, and PLT@Ag-MOF-Vanc. (f) FTIR spectra of Ag-MOF, 2-methylimidazole and AgNO3.

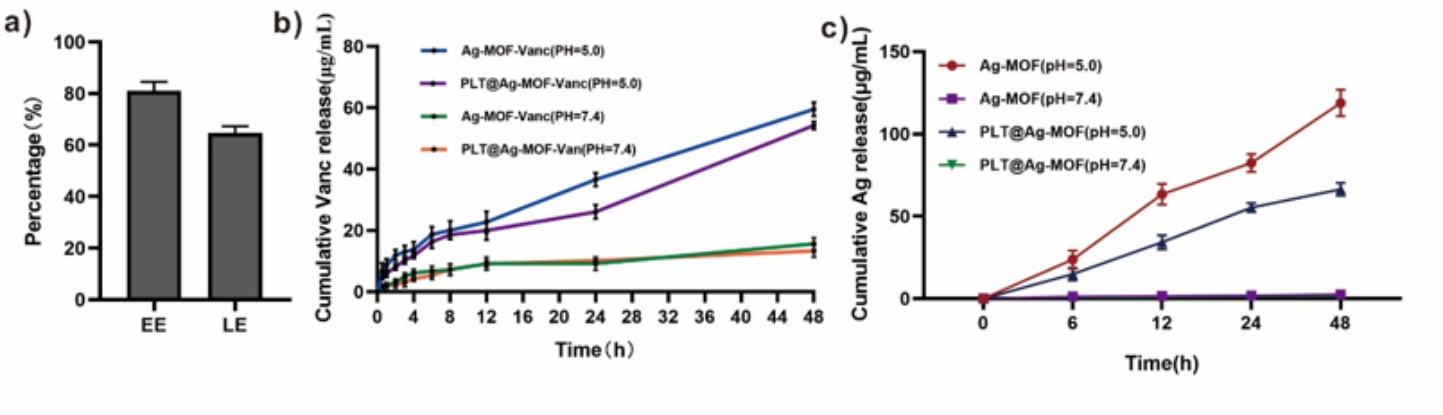

Figure 3

Drug loading and release of PLT@Ag-MOF-Vanc. (a) EE and LE of PLT@Ag-MOF-Vanc. (b) Cumulative release rates of Vanc from Ag-MOF-Vanc or PLT@Ag-MOF-Vanc at different pH values (5.0 and 7.4). (c) Cumulative release rates of Ag+ from Ag-MOF-Vanc or PLT@Ag-MOF-Vanc at different pH values (5.0 and 7.4).

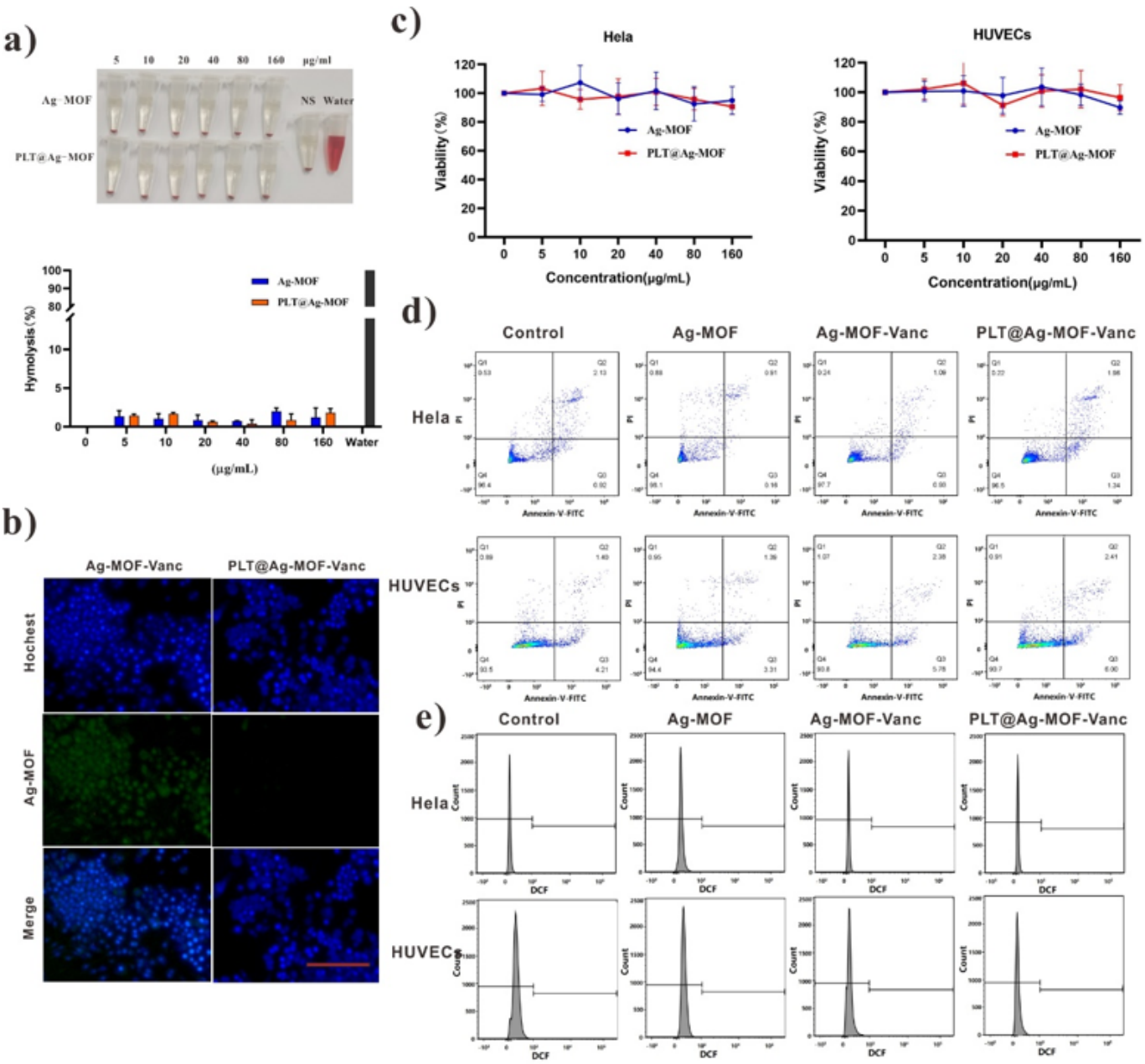

Figure 4

Biocompatibility of PLT@Ag-MOF-Vanc. (a) Images and hemolytic ratios of erythrocytes' suspensions after treatment with different doses of Ag-MOF or PLT@Ag-MOF. (b) LCFM images of RAW264.7 cells upon culture with Ag-MOF-Vanc or PLT@Ag-MOF-Vanc for 24 h. Scale bar:100 μm. (c) Cell viability of HeLa and HUVECs cells treated with various concentrations of Ag-MOF and PLT@Ag-MOF based on CCK-8 test. (d) Apoptosis assessed by flow cytometry in HeLa cells and HUVECs previously treated with Ag-MOF, Ag-MOF-Vanc, or PLT@Ag-MOF-Vanc for 48 h. (e) ROS level evaluation by flow cytometry in HeLa cells and HUVECs treated with Ag-MOF, Ag-MOF-Vanc, or PLT@Ag-MOF-Vanc for 48 h.

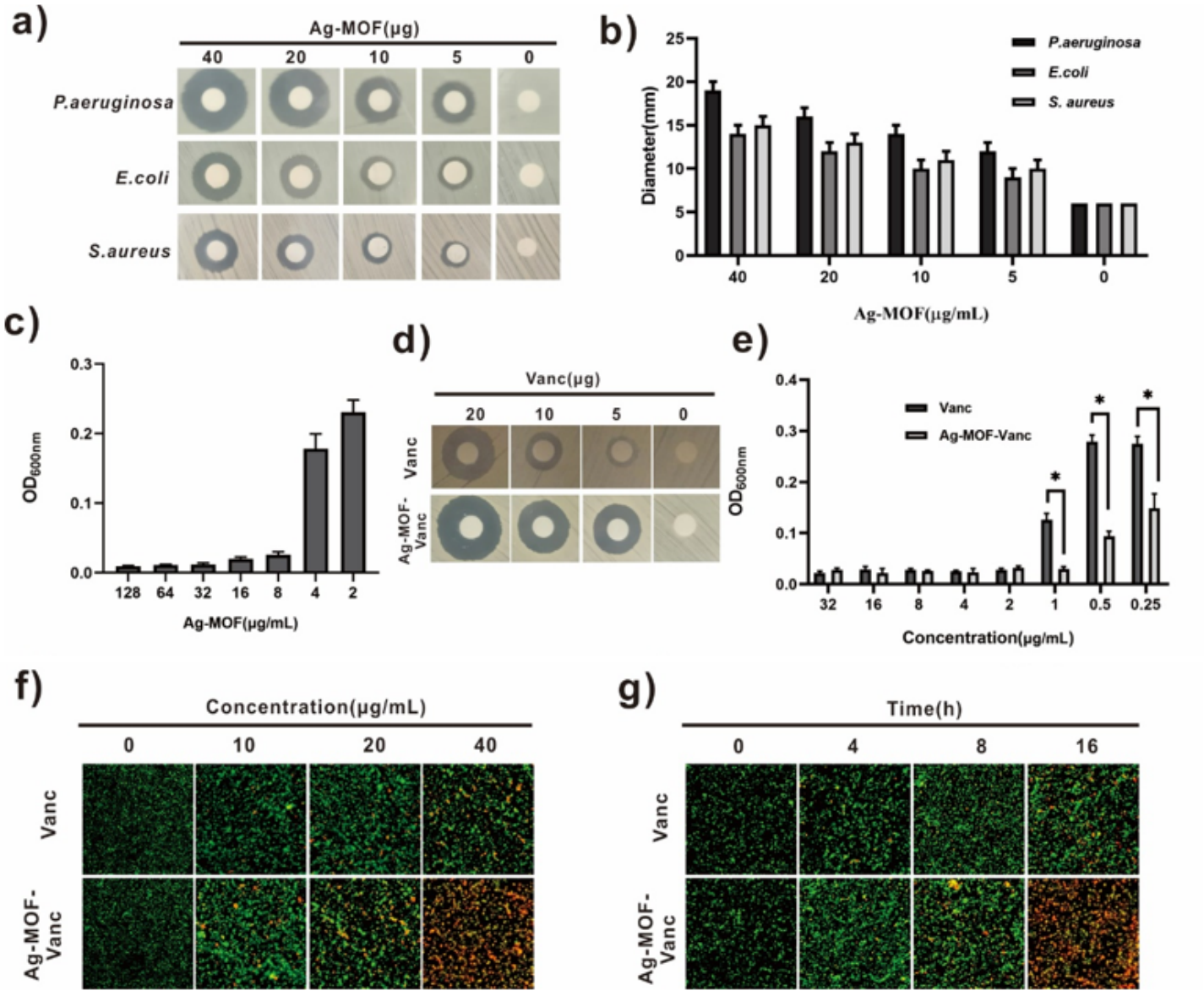

Figure 5

In vitro antibacterial effect of Ag-MOF-Vanc. (a) Inhibition zones and (b) corresponding inhibition zone diameters (cm) of Ag-MOF against different bacteria. (c) Concentration effects of Ag-MOF on the growth of MRSA. (d) Inhibition zones and (e) concentration effects of Vanc or Ag-MOF-Vanc against MRSA. (f) Confocal imaging of death/live staining after exposing MRSA to varying concentrations of Vanc or Ag-MOF-Vanc. (g) Confocal imaging of death/live staining after MRSA exposure to Vanc or Ag-MOF-Vanc with different incubation time. Scale bar:20 μm. * $p < 0.05$.

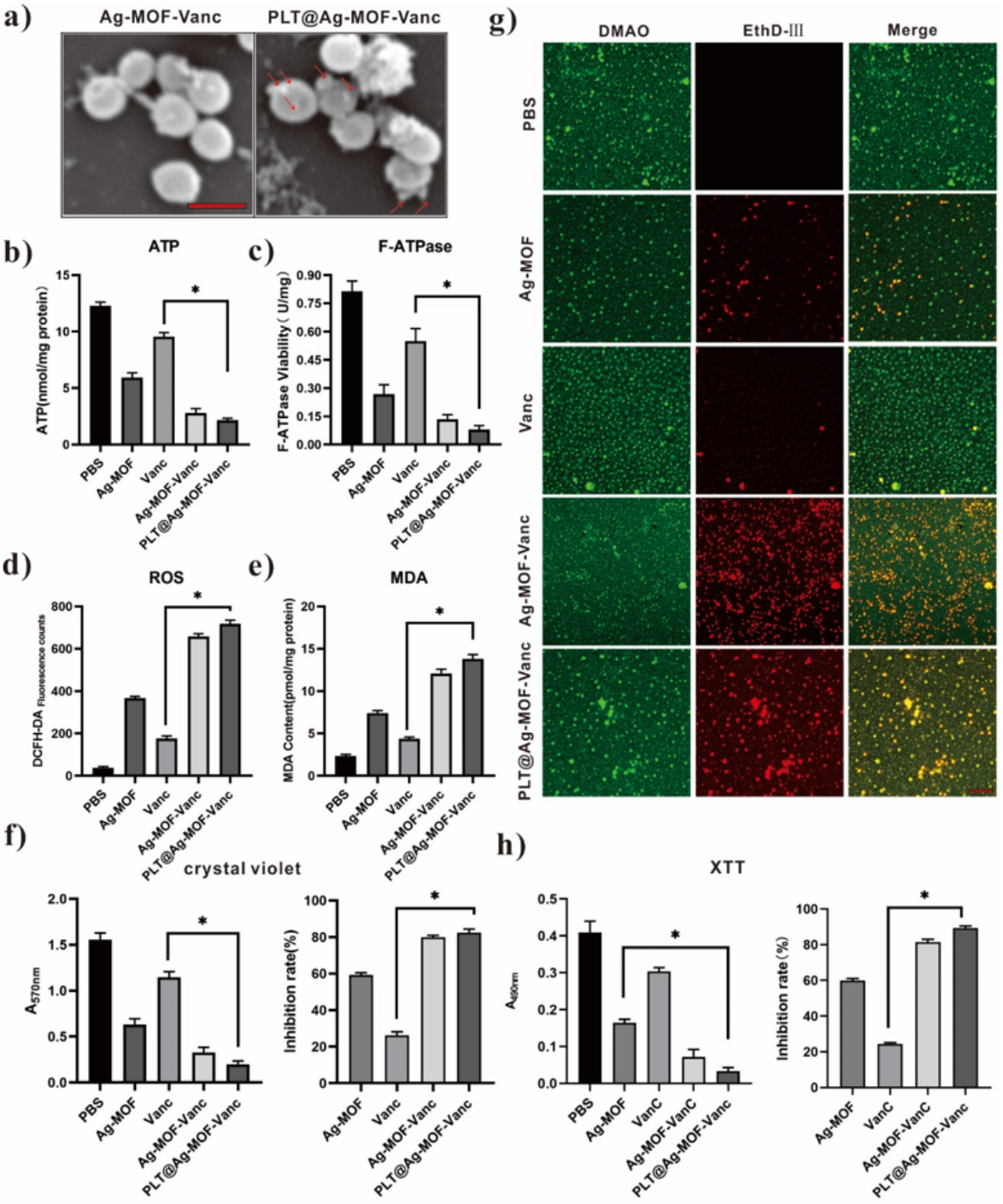

Figure 6

Antibacterial mechanism of PLT@Ag-MOF-Vanc. (a) SEM images of MRSA incubated with Ag-MOF-Vanc or PLT@ Ag-MOF-Vanc. Scale bar:1 μm (b) Intracellular ATP level, (c) F-type ATPase activity, (d) DCFH-DA fluorescence counts, and (e) MDA contents of MRSA treated with Ag-MOF, Vanc, Ag-MOF-Vanc, or PLT@ Ag-MOF-Vanc. (f) Crystal violet staining, (g) laser confocal microscopy, and (h) XTT dyeing of MRSA biofilm. Scale bar:20 μm. * $p < 0.05$.

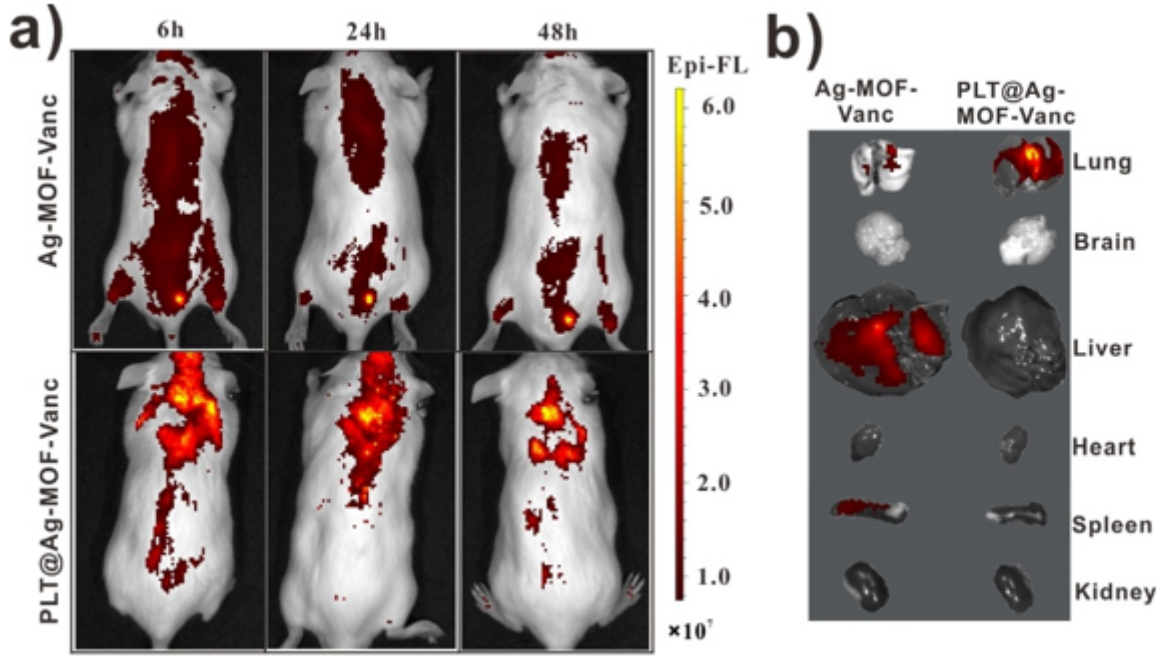

Figure 7

In vivo targeting potential of PLT@Ag-MOF-Vanc. (a) In vivo fluorescence images of Kunming mice at 6, 24, and 48 h upon intravenous treatment with Cy5-labeled Ag-MOF-Vanc and Cy5-labeled PLT@Ag-MOF-Vanc. (b) Ex vivo bioluminescence images of visceral organs and tumors at 48 h after treatment with Cy5-labeled Ag-MOF-Vanc and Cy5-labeled PLT@Ag-MOF-Vanc.

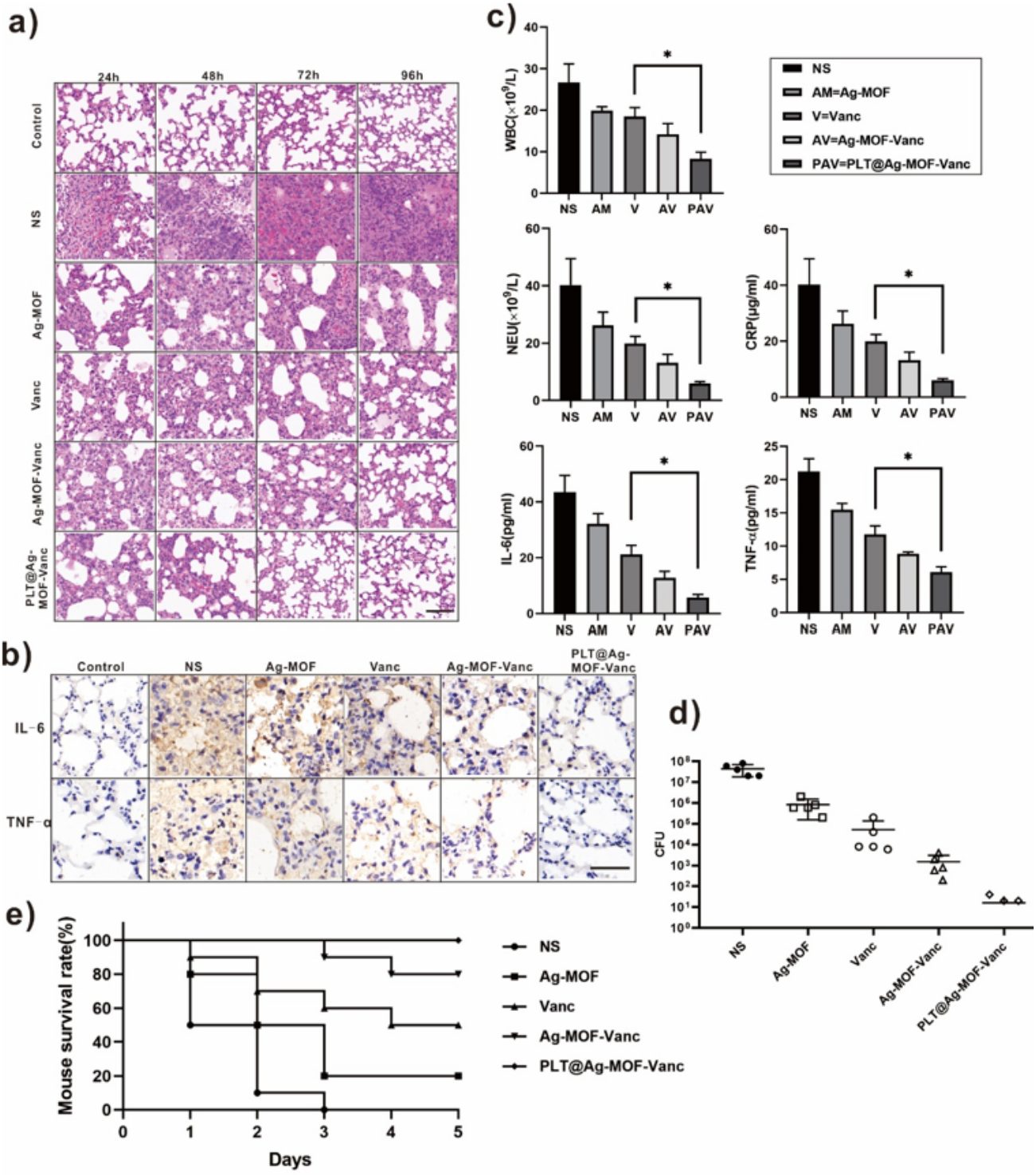

Figure 8

Anti-infection effect of PLT@Ag-MOF-Vanc in vivo. (a) HE staining images of lung tissues. (b) Immunohistochemical staining of IL-6 and TNF-α in lung tissues. (c) Inflammation-associated cell counts and cytokine levels in the blood. (d) Bacterial count in alveolar lavage fluid. (e) Survival rates in the mouse MRSA pneumonia model after different treatments. Scale bar:100 μm. * $p < 0.05$.

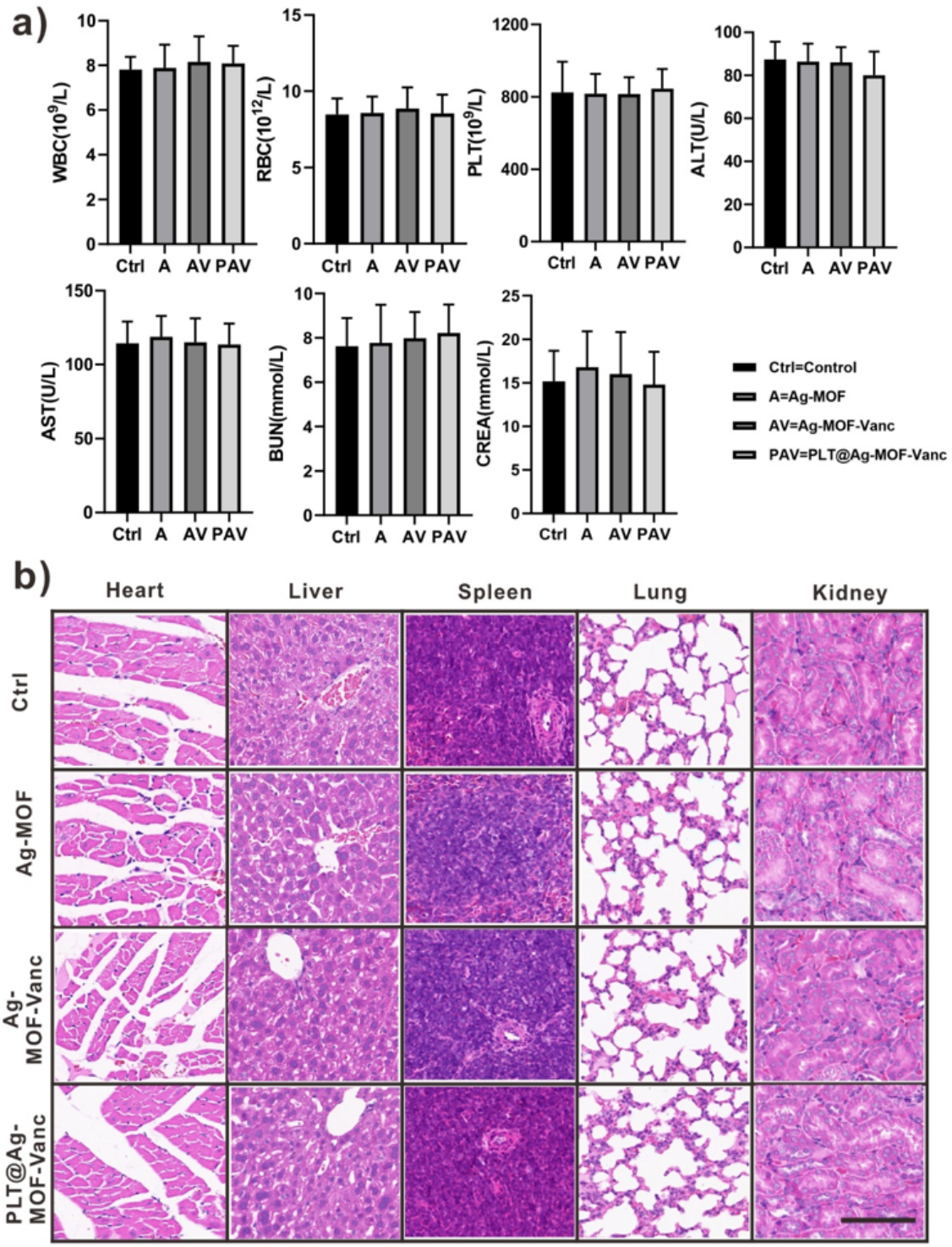

Figure 9

In vivo toxicity assessment of PLT@Ag-MOF-Vanc. (a) CBC and serum indexes in mice at 1 week after intravenous injection of Ag-MOF, Ag-MOF-Vanc, and PLT@ Ag-MOF-Vanc. (b) Histological images of heart, liver, spleen, lung, and kidney samples from mice at 1 week after intravenous injection of Ag-MOF, Ag-MOF-Vanc, and PLT@ Ag-MOF-Vanc. Scale bar:100 μm.